

# Optimal Magnetorquer Rod Design for Small-Size Satellites using Axiomatic Design Theory and Nanocrystalline Material Core

Luiz de Siqueira Martins-Filho<sup>1</sup> , Matheus de Almeida Soares<sup>2</sup> , Eduardo Gueron<sup>1</sup>, Eduardo dos Santos Ferreira<sup>1</sup> , Hérlon de Oliveira Morsch<sup>3</sup>

1. Universidade Federal do ABC  – Centro de Engenharia, Modelagem e Ciências Sociais Aplicadas – São Bernardo do Campo/SP – Brazil.

2. Horuseye Tech Engenharia de Sistemas Ltda – São José dos Campos/SP – Brazil.

3. Magmattec Tecnologia em Materiais Magnéticos Ltda – Cachoeirinha/RS – Brazil.

\*Correspondence author: [luiz.martins@ufabc.edu.br](mailto:luiz.martins@ufabc.edu.br)

## ABSTRACT

The magnetic torquer rod, also called a magnetorquer, is the most popular actuator for attitude control of satellites in low Earth orbit. In the case of nano and picosatellites, the available inner space is quite limited, as is the maximum power value. An optimal design solution is highly desirable to produce adequate torque while minimizing energy consumption and mass. Based on the axiomatic design theory, a solution was developed by establishing the requirements – wire diameter, magnetic dipole moment, voltage, and solenoid length – and the physical domain variables – number of turns, current, resistance, and wire length. As a result of the modelling, the design system is decoupled. The choice of core material can also contribute to the actuator's improvement. Two options are proposed in this work: the FINEMET, a nanocrystal composed of various metals and other elements, and the FeNi50 alloy, for comparative performance. In terms of design parameters, four prototypes were developed to evaluate different wiring configurations and two core materials. The test results of the design options reveal a contrasting performance concerning core material: while the utilization of nanocrystalline material yields superior hysteresis characteristics or linearity behavior, the FeNi50 alloy exhibits enhanced magnetization magnitude.

**Keywords:** Nanosatellites; Attitude control; Magnetorquer rod; Axiomatic design; Design optimization.

## INTRODUCTION

The trend toward miniaturization in mechatronic systems, propelled by advancements in microelectronics and micro-electro-mechanical systems (MEMS) technology, has permeated the aerospace domain, finding its expression in the realm of drones and small-scale satellites. Notably, nano and picosatellites have surged in popularity over recent decades, spurred by the standardization set forth for CubeSats (Cal Poly 2020). This surge has instigated substantial efforts to enhance the sophistication of these spacecraft, thereby broadening their spectrum of applications and mission profiles. This technological evolution has, in turn, ushered in greater accessibility to space through academic programs and private sector initiatives, creating a promising dynamic in the space industry and market, as discussed by Perondi (2023) and Pessoa-Filho (2021).

**Received:** Apr 03 2024 | **Accepted:** Jun 14 2024

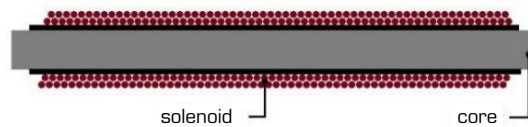
**Section editor:** Alison Moraes 

**Peer Review History:** Single Blind Peer Review.



Examples of these efforts to develop missions and devices involving CubeSats include projects such as the design of two satellites for a technological competition by the Instituto Nacional de Telecomunicações (Inatel) (Coutinho *et al.* 2023) and the development of a fault-tolerant attitude determination system by a group of researchers from Brazilian public universities (Duarte *et al.* 2020).

The precise control of satellites' orientation is crucial for their effective functioning. This is achieved through careful management of their attitude. Certain missions depend on achieving precise spatial orientation (i.e., attitude) as a paramount prerequisite for the effective operation of their payloads. For instance, the quality of Earth's surface imaging data is contingent upon maintaining stable and accurate pointing of the camera imager. To attain such precision in attitude control, the vehicle's navigation systems must incorporate a robust and highly accurate attitude determination and control system (ADCS) (Markley and Crassidis 2014). One of the commonly favored actuation mechanisms for satellite attitude control is the magnetorquer rod, which comprises a solenoid, optionally equipped with a core. This ingenious device interacts with the Earth's geomagnetic field when an electric current traverses its wire (Fig. 1).



Source: Elaborated by the authors.

**Figure 1.** A magnetorquer rod scheme including a solenoid and a core.

The exploration of the interplay between the Earth's geomagnetic field and spacecraft, along with the development of magnetic-based attitude control devices and actuators aimed at technological enhancement – such as precision enhancement, dimension and mass reduction, and energy consumption reduction – embarks on a historical journey that has spanned the entire course of space exploration. This enduring pursuit is underscored by notable milestones, including a technical report on spacecraft dipole moment interaction with the geomagnetic field published by the National Aeronautics and Space Administration (NASA 1969), and a comprehensive study on torque rod design conducted by the Lincoln Lab/Massachusetts Institute of Technology (MIT) in 1965.

In more recent contributions to this field, Carrara and Varotto (1995) meticulously charted a roadmap for the design of magnetorquer rods, considering both free-air solenoid and ferromagnetic core configurations. The holistic endeavor encompassing the design, manufacturing, and testing of high-capacity magnetic torque actuators for attitude control was addressed by Lee *et al.* (2005). Meanwhile, Mehrjardi and Mirshams (2010) ventured into the realm of mathematical modeling-based design algorithms for magnetic torquers, selecting the CK30 alloy as their solenoid's soft magnetic core material.

Farrahi and Sanz-Andrés (2013) introduced a method for evaluating the damping efficiency of hysteresis rods aboard small satellites, exploring various ferromagnetic materials and distinct rod shapes, including thin film and traditional circular cross-sections. Furthermore, research into hysteresis damper devices for passive magnetic attitude control systems, where the rods exert damping torque to curtail satellite angular momentum and angular velocity, was presented by Ousaloo (2013). Throughout these studies, the pivotal requirements for magnetorquers in the context of CubeSats invariably revolve around dimensions, weight, and magnetic characteristics, essentially encapsulating operation energy consumption, magnetic dipole moment generation, and actuator response linearity.

Our endeavor serves a dual purpose: to advance the design of magnetorquer rods for small satellites through optimized solutions grounded in axiomatic design theory (Suh 1990), and to introduce the utilization of a nanocrystalline soft magnetic alloy, namely FINEMET from Hitachi Metals Ltd. (2016), as a solenoid core material. As a result, we can highlight that the contributions of this work lie in applying a well-established design technique from diverse fields to the specific problem of designing magnetic actuators for satellites. Additionally, it involves the utilization of an innovative material that offers attractive performance for addressing this particular issue. This choice is poised to enhance the magnetic behavior of the attitude actuator.

## Magnetism of magnetorquer rods

The attitude actuation of a magnetorquer rod results from the interaction between the magnetic dipole moment of the device and the geomagnetic field. Therefore, the actuator produces a torque in the satellite body around its center of gravity. This torque is expressed by:

$$\tau = m \cdot B \quad (1)$$

where  $m$  is the magnetic dipole moment (in  $\text{Am}^2$ ) and  $B$  is the magnetic flux density or induction magnetic (in T or N/Am) (Feynman *et al.* 2012; Markley and Crassidis 2014).

Considering a constant geomagnetic field, the produced torque magnitude depends directly on the direction and magnitude of the rod's magnetic dipole moment. This moment's magnitude results from the core material, the core dimensions, and the solenoid characteristics (number of turns, number of layers, wire material, and wire gauge). A solenoid can alternatively be without a core, or in short, a free-air solenoid. The core is usually made of a ferromagnetic material, which has convenient magnetic properties when exposed to a magnetic field.

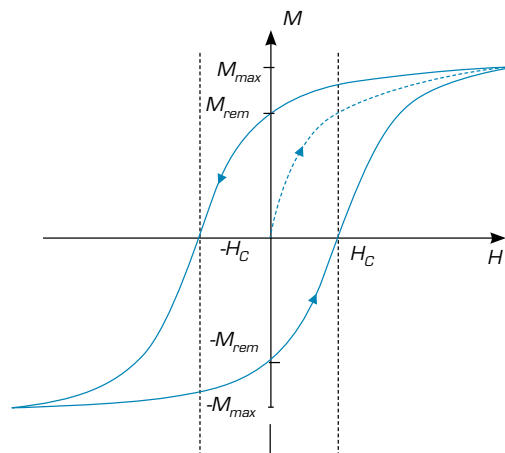
According to Ampere's law of induction, the magnetic field generated by a typically long solenoid is (Feynman *et al.* 2012):

$$B = \mu_0 \cdot n \cdot I \cdot L \quad (2)$$

where  $n$  is the number of turns,  $I$  is the current in A,  $L$  is the length of the solenoid in m, and  $\mu_0$  is the magnetic field in A/m. The produced magnetic field is oriented in the axial direction of the solenoid. The long rod model is the one where the magnetic field outside the solenoid is much weaker than inside and can be disregarded. To simplify the calculations, the magnetic field lines at the solenoid extremities are omitted.

Considering a ferromagnetic material core, the magnetic properties are intensified and the magnetic dipole moment is increased. However, an undesirable phenomenon occurs: a magnetic hysteresis cycle is generated in the core. The relationship between magnetic flux density and the magnetic field is not linear and is also dependent on the time evolution of the material's magnetization process.

The hysteresis loop diagram is illustrated in Fig. 2 (Ousaloo 2013). This curve for a material is usually characterized by three parameters: the maximum magnetization  $M_{\max}$ , the remaining magnetization after removal of the external field  $M_{\text{rem}}$ , and the magnetic field required to nullify the magnetization  $H_c$ .



Source: Adapted from Ousaloo (2013).

**Figure 2.** The hysteresis diagram.



In the saturation zone of the hysteresis, the induction can be estimated by (Santoni and Zelli 2009):

$$B = \frac{\mu_0 \cdot H}{1 + \frac{H}{H_c}} \quad (3)$$

where  $\mu_0$  is the vacuum magnetic permeability,  $H$  is the magnetic field parallel to the solenoid, and  $H_c$  is the material apparent permeability that can be related to the true permeability  $\mu$ . The apparent permeability at saturation is given by:

$$\mu_a = \frac{\mu}{1 + \frac{M_{rem}}{M_{max}}} \quad (4)$$

where  $\mu_a$  is the apparent permeability, and  $M_{rem}$  and  $M_{max}$  are the remaining and maximum magnetization, respectively.

For a rectangular core, the demagnetizing factor in the axial direction of the rod is given by (Sato and Ishii 1989):

$$N_z = \frac{l_{minor}}{l_{major}} \quad (5)$$

where  $l_{minor}$  is the rod minor length, and  $l_{major}$  is the rod major length. The length of the solenoid is not necessarily the same as that of the core. In this study, the core is considered longer than the solenoid.

The magnetic dipole moment in saturation can be modeled by (Gerhardt and Palo 2010):

where  $V$  is the core volume.

$$m = \frac{\mu_a V}{l_{minor}} \quad (6)$$

The current is the variable to achieve the magnetic moment expressed by Eq. 4. It depends on the number of turns, which can be determined. The number of turns is proportional to the number of layers,  $n_l$ , i.e.:

$$n_t = n_l \cdot n_{layer} \quad (7)$$

where  $n_l$  is the number of turns per layer. This term expresses how many turns are possible for each layer and depends on the ratio of the length of the solenoid to the wire's diameter,

$$n_{layer} = \frac{l_{layer}}{d} \quad (8)$$

The diameter of the wire is defined based on the American Wire Gauge (AWG) table, which relates each copper wire gauge with its main physical characteristics as diameter, mass, resistance, maximum current, and maximum operating temperature. According to ASTM B258- 18 (2018), Copper 100 IACS has density of  $\rho = 8.89 \times 10^6 \text{ g}\cdot\text{m}^{-3}$  and resistivity of  $\rho_r = 0.153 \text{ } \Omega \cdot \text{g}\cdot\text{m}^{-2}$ . The relative mass is calculated using:

$$m_r = \frac{\rho_r \cdot d^2}{4} \quad (9)$$

and relative resistance,

$$R_r = \frac{4 \cdot \rho_r \cdot l}{\pi \cdot d^2} \quad (10)$$

Considering the solenoid geometry, the dependence between the number of turns and the number of complete winding layers, and the wire length dependence of the layer diameter, the resulting length of wire for a square section prismatic core can be obtained by:

$$L_{wire} = n_t \cdot l_{layer} + (n_t - 1) \cdot l_{overlap} \quad (11)$$

where  $l_{layer}$  is the intern width of the solenoid, i.e., is the width where the first layer will be rolled.

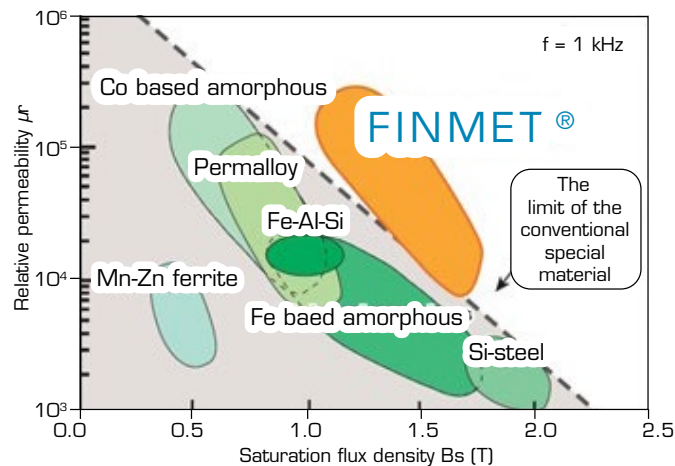
### Magnetorquer rod design

The methodology employed for developing the magnetic torque device includes the following steps:

- Selection of solenoid core material – Two distinct materials, namely the FINEMET nanocrystalline material and the FeNi50 alloy, are tested to assess the linearity characteristics of device actuation and the magnitude of magnetization generated during actuation.
- Definition of device design parameters – Various dimensions, wire gauge for winding, number of turns, and winding layers are established. Given the interconnected nature and mutual dependence of these parameters, the axiomatic design theory is adopted to establish systematic criteria for selection. Four combinations are chosen based on the parameter dependence surfaces derived using the principles of axiomatic design theory.
- Prototype construction – This involves the manufacturing of spools, assembly of cores, and winding of wires to create appropriate devices for conducting comparative performance tests of the different models.
- Testing of devices – Voltage is applied to the solenoid and the generated magnetic field is measured. A complete cycle of positive and negative voltage values is considered to evaluate the resulting hysteresis curve.
- Results analysis – Preliminary test results of the tests are described in graphs to highlight the linearity of the drive, and the main magnetic actuation parameters are calculated, including the field and magnetization in the longitudinal and transverse directions to the device.

The first core material proposed is the FINEMET soft magnetic alloy (Hitachi 2016), a thin nanocrystal composed of metallic elements Fe, Cu, and Nb, as well as B and Si. The manufacturer aimed to obtain a better combination of permeability and magnetic flux density saturation compared to other metal alloys. This nanocrystalline material choice aims to test innovative device design for performance improvement.

According to Gheiratmand and Hosseini (2016), research on magnetic materials for varied applications, after decades of predominance of steel alloys containing silicon used in various laminated products and cores for small motors, large power distribution transformers, and even for electric motors and generators, has recently turned to soft nanocrystalline magnetic alloys. The specific case of FINEMET has attracted great interest and become the focus of several studies due to its magnetic properties and advantageous characteristics compared to amorphous or crystalline alloys (e.g., high magnetic saturation, high permeability, low core loss). Comparative characteristics of FINEMET and other soft magnetic materials are shown in Fig. 3.



Source: Hitachi Metals Ltd. (2016).

**Figure 3.** Relationship between relative permeability and magnetic flux saturation density of various soft magnetic materials.



Three different configurations of solenoid wiring (wire gauge, number of turns in the coil) resulted in three prototypes developed using the FINEMET core. This material core has a square section due to the constructive procedure (a bar composed of several layers of thin strip). The performance of the magnetorquer in terms of the core material choice is also tested by comparing it with another material. The design of FINEMET core prototypes was adapted to an alternative version using the FeNi50 alloy (Schaeffer and Espinoza 2000) as the core. This material has a circular cross-section bar shape.

Axiomatic design is a method developed to make appropriate design decisions for a product, a system, a process, or a service (Suh 1990). For a product, the purpose of this method is to provide the best model to generate a quality product, i.e., a product that satisfies the design specifications proposed by customers (Suh 1995).

The axiomatic design specifies four domains:

- Customer domain (CA): customer requirements and specifications for the product;
- Functional domain (FR): functional requirements of the product as specified by customers;
- Physical domain (DP): physical formulation to achieve the functional requirements;
- Process domain (PV): manufacturing methods to control the physical domain.

To guarantee the best solution, Suh (1995) proposed two axioms:

- Independence axiom: FR are independent and the design process needs to maintain this independency.
- Information axiom: if there is more than one design that satisfies axiom 1, the best design is the simplest, the one with the least information.

The design is a decomposition task alternating between **FR** and **DP** domains: when a **FR** is set, it is firstly necessary to define a series of **DP** that meet this **FR**. Then another **FR** can be set. The functional requirements are defined as a vector **F** and the physical domain as a vector **D**. They are related by:

$$[\mathbf{D}] = [\mathbf{M}] [\mathbf{F}] \quad (12)$$

where **[M]** is the design matrix relating each FR to its DP. When **[M]** is diagonal, each FR is related to just one DP, and then it is called uncoupled design. This case is considered as the ideal model. When **[M]** is triangular, the first FR is the most important and its definition influences all the other ones. This model is called decoupled design and yet satisfy the first axiom. If **[M]** has any form, the model is considered as coupled design and does not satisfy the first axiom. In this case, the **FR** must be changed. The elements of **[M]** consist of *X* and 0: *X* is set in position *i, j* when the *i*<sup>th</sup> **FR** is related to the *j*<sup>th</sup> **DP** and 0 is set when there is no relation between domains.

The product design begins with the customer requirements. According to Roohnavazfar *et al.* (2014), the minimum functional requirements expressing the customer domain must be defined in terms of technical-scientific relations. The initial requirements relate to the device dimensions: the small space inside a CubeSat restricts the dimensions of the torquer rod device. In terms of electrical powering, the usual available voltage is 5 V. Considering the magnetorquers in the market, an adequate actuator should produce a dipole moment around 0.2 Am<sup>2</sup>. The core of the first prototypes was defined as a rectangular FINEMET bar with dimensions 9.5 × 9.5 × 100 mm. The bar is made up of several layers of FINEMET strip (the original presentation of this material). In the future, the bar dimensions would be smaller, possibly 7.5 × 7.5 × 80 mm, after overcoming difficulties in cutting and machining the original tape. The nominal relative magnetic permeability is 80000 N/A<sup>2</sup>. There is a minimum of 1 layer, but a maximum of 15 is fixed to minimize mass. The wire diameter is chosen to be in the range between AWG 25 and 33, considering the characteristics of the automated rolling process. Expressing customer domain in functional requirements (FR): (**FR**<sub>1</sub>): *d* = wire diameter (mm) varies between 0.180 and 0.455 mm; (**FR**<sub>2</sub>): *m* = magnetic dipole moment (Am<sup>2</sup>) must be 0.2 Am<sup>2</sup>; (**FR**<sub>3</sub>): *V* = tension (V) must be 5 V; (**FR**<sub>4</sub>): *l* = solenoid length (mm) must be 90 mm. Other constraints can be fixed for calculus: number of layers: *n*<sub>l</sub> between 1 and 15; core length: *l*<sub>c</sub> = 100 mm; core width: *w*<sub>c</sub> = 9.5 mm; relative magnetic permeability: *μ*<sub>r</sub> = 80000 N/A<sup>2</sup>; solenoid intern width: *w*<sub>s</sub> = 13.5 mm.

Once defined FR, it is necessary to define the relatives DP to achieve each of them, alternating between these domains. Considering Eqs. 13 and 14, to satisfy FR<sub>2</sub>, it is necessary to calculate the number of turns *n*<sub>t</sub> and the first DP is defined as:

$$n_t = \frac{1}{\mu_r} \cdot \frac{l_c}{l_s} \cdot \frac{m}{B} \quad (13)$$

In order to satisfy the second functional requirement, electrical current is the second DP, calculated from Eqs. 2-6, resulting in:

$$I = \frac{m}{n_t \cdot A_s \cdot B} \quad (14)$$

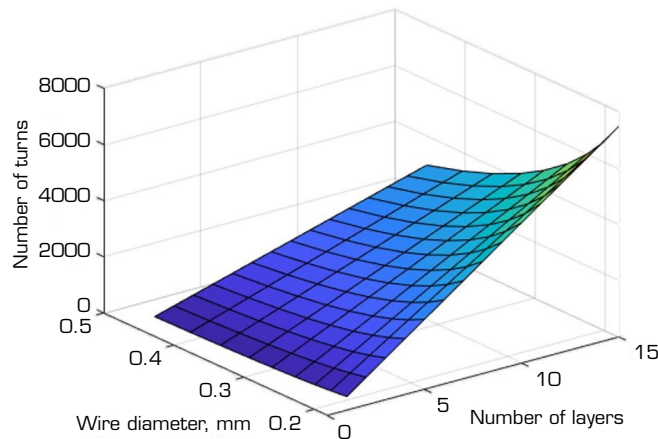
where it is clear that  $n_t$  must be defined first than  $I$ . To achieve FR<sub>1</sub>, resistance of solenoid must be calculated as indicated in Eq. 11, becoming the third DP. Finally, considering Eq. 11, the fourth DP is the wire length  $L_w$  to satisfy the solenoid length.

The relation between FR and DP, expressed by Eq. 15, becomes:

$$\begin{pmatrix} d_{wire} \\ m \\ U \\ l_{sol} \end{pmatrix} = \begin{pmatrix} \blacksquare & 0 & 0 & 0 \\ \blacksquare & \blacksquare & 0 & 0 \\ 0 & \blacksquare & \blacksquare & 0 \\ 0 & 0 & \blacksquare & \blacksquare \end{pmatrix} \begin{pmatrix} n \\ I \\ R \\ l_{wire} \end{pmatrix} \quad (15)$$

where the symbol ( $\blacksquare$ ) denotes the dependence between the parameters.

This relationship allows the model to be classified as a decoupled design without violating the first axiom. Thus, one examines the interdependence of the parameters in this model. Figures 4-7 represent graphical results in the form of surfaces. These surfaces can guide design decisions; for instance, selecting a value for one parameter may restrict the available options for others, as illustrated in the graphical representations. Figure 4 represents the number of turns. The number of turns reaches the minimum value when the wire diameter is the largest one, but it is maximum for a greater number of layers. The maximum value of turns is related to the maximum number of layers. For a fixed number of layers, the number of turns decreases when the wire diameter is increases.

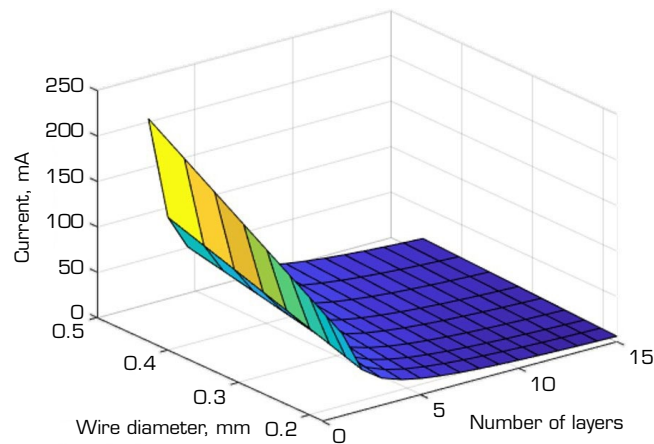


Source: Elaborated by the authors.

**Figure 4.** Number of turns as a function of number of layers and wire diameter.

In Fig. 5, the current reaches the maximum value when the wire diameter is the largest and the number of layers is the smallest. As the wire diameter increases, the sectional area and consequently the electron density per unit area also increases. Therefore, the electrical current needs to be increased since more electrons need to be induced. The current diminishes as the number of layers increases because less current per layer is necessary to achieve a determined value of the magnetic field.

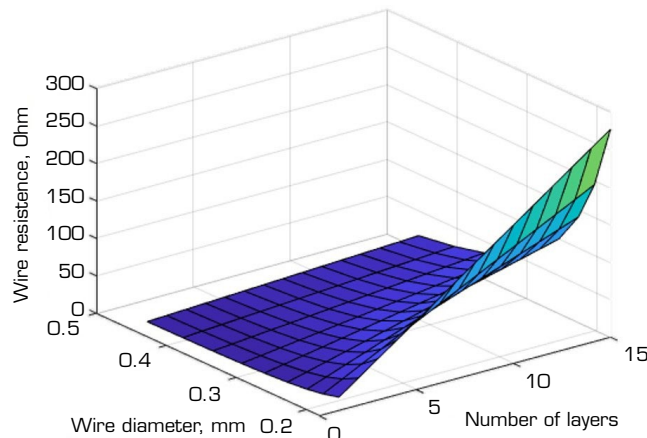




Source: Elaborated by the authors.

**Figure 5.** Current as a function of number of layers and wire diameter.

Figures 6 and 7 illustrate the variations in resistance and wire length, respectively, based on changes in the number of layers and wire diameter. They exhibit the same behavior as the number of turns represented in Fig. 5. As the number of layers increases, more wire is required for winding, leading to an overall increase in total resistance due to increased wire length. Conversely, as the wire diameter increases, fewer turns are needed per layer, reducing the amount of wire required and thereby lowering wire resistance.



Source: Elaborated by the authors.

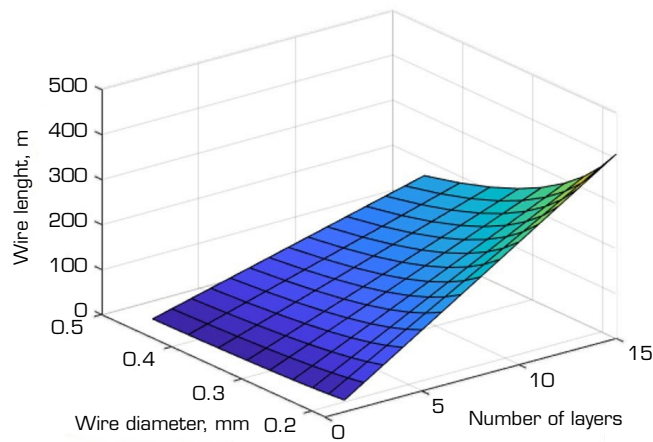
**Figure 6.** Wire resistance as a function of number of layers and wire diameter.

To solve this problem using axiomatic theory, some constraints need to be set. However, the magnetic field generated by the solenoid and saturated induction are fixed by the model. The magnetic field is 1005 A/m and saturated induction is 27.8 mT for any value of certain DP.

To validate the design, a prototype was built with wire AWG 30 and 5 layers. Details of the first three manufacturing steps of this prototype (T0100-1) can be seen in Fig. 8. The number of turns was counted by a specialized rolling machine and the wire length was estimated by comparing magnetorquer's weight before and after rolling the wire using relative mass.

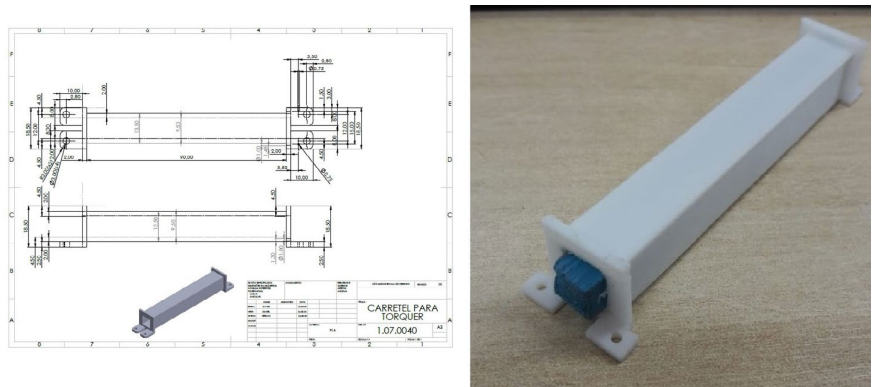
Upon setting the wire diameter and the number of layers for the prototype, the resulting manufactured prototype is slightly different from the designed prototype (Table 1). The designed number of turns has 10.6% more turns than the manufactured one. Consequently, there is a decrease of 7.89% in wire length. This difference results from the characteristics of the rolling machine used in the manufacturing process.





Source: Elaborated by the authors.

**Figure 7.** Wire length as a function of number of layers and wire diameter.



Source: Elaborated by the authors.

**Figure 8.** The drawing of the frame for the coil wiring and the torquer device assembled with core read for wiring.

**Table 1.** Comparison between properties of designed and manufactured magnetorquer prototype with wire AWG 30 and 5 layers.

Property	Manufactured	Designed
Number of turns	1,600	1,770
Current for 5V, mA	56.5	51.1
Resistance for 5V, Ω	88.4	97.8
Wire length, m	90.0	97.1

Source: Elaborated by the authors.

Based on the proposed device design methodology, a series of three models was defined. The last model, to allow comparison with another core material, the FeNi50 alloy, has a second version with small differences in dimensions because this core has a cylindrical shape (a consequence of the manufacturing process, where it is impossible to machine to reduce the diameter without losing its magnetic characteristics). The prototype specifications could not always be exactly obtained by the available manufacturing process. These parameters, already adjusted after being measured in the laboratory, are shown in Table 2.

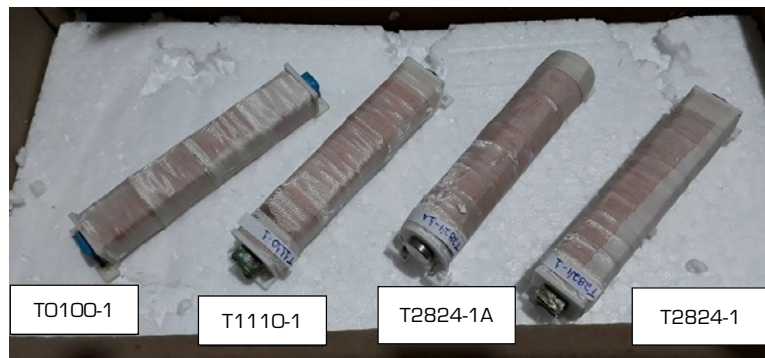


**Table 2.** The designing parameters of the four prototypes of magnetorquer rods.

Prototype	Number of spirals	Resistance (ohm)	AWG (wire gauge)	L solenoid (mm)
T0100-1	1,000	10.0	26	90
T1110-1	1,600	33.0	30	90
T2824-1	2,500	47.6	30	90
T2824-1A	2,500	50.0	30	90

Source: Elaborated by the authors.

The produced prototypes of the torquer rods are shown in Fig. 9: T0100-1 (FINEMET core), T1110-0 (FINEMET core), T2824-1A (FeNi50 core), and T2824-1 (FINEMET core).



Source: Elaborated by the authors.

**Figure 9.** The four prototypes considered in the experimental tests.

The total mass of each prototype (plastic structure, winding, core, and connectors) is, respectively, 92.7 g for T0100-1, 124.8 g for T1110-1, 148.9 g for T2824-1A, and 127.9 g for T2824-1.

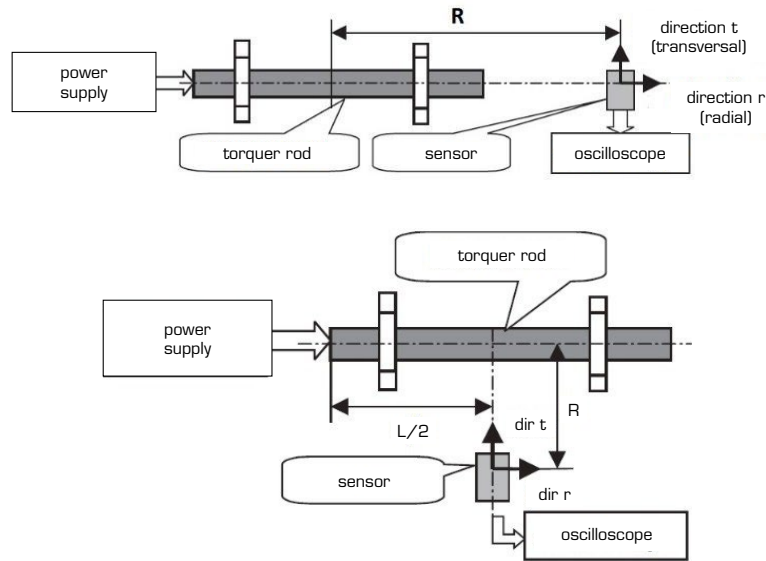
## RESULTS AND DISCUSSION

The experimental setup for testing the prototypes is adapted from the methodology proposed by Lee *et al.* (2002). The magnetic field is generated by the magnetorquer upon the application of voltage to the solenoid. This evaluation consists of a complete cycle of both positive and negative voltage values to assess the resulting hysteresis curve.

Two distinct configurations were employed for magnetic field measurements, as illustrated in Fig. 10. Measurements are conducted in both the radial (or longitudinal) direction and the transversal direction, with the sensor probe positioned at distances  $R_r$  and  $R_t$  from the geometric center of the magnetorquer, respectively. For these measurements, an accurate magnetometer manufactured by SenSys GmbH model FGM3D/250 (SenSys Sensorik & Systemtechnologie GmbH) was employed.

Table 3 presents a summary of the preliminary test results for the magnetorquer prototypes, including the maximum magnetization values of the coils. Notably, the results reveal a considerable disparity between the radial and transverse directions concerning both field strength and magnetization. Specifically, the field strength and magnetization are significantly higher along the radial direction, aligned with the coil axis, suggesting an effective concentration of the magnetic field by the core. This observation indicates that the device performs as expected for a torquer rod.

The magnetic field and magnetization measurements in the radial and transverse directions for the four prototypes can be seen in Figs. 11–14: the radial field, the magnetization in the radial direction, the transverse field, and the magnetization in the transverse direction.



Source: Adapted from Lee et al. (2002).

**Figure 10.** Radial and transversal setups for measurement of magnetic field generated by the torquer rod devices.

**Table 3.** Summary of test results.

Prototype	Rr (mm)	Rt (mm)	Br (uT)	Bt (uT)	Ib (mA)
T0100-1	109.5	64.5	120	20	99
T1110-1	109.5	64.5	110	28	110
T2824-1	109.5	64.5	142	35	77
T2824-1A	109.5	65.5	185	44	77
Prototype	Mr (Am <sup>2</sup> )	Mt (Am <sup>2</sup> )	M (Am <sup>2</sup> )	θ	Ind. (H)
T0100-1	0.4493	0.0973	0.4597	12.2	0.7
T1110-1	0.4119	0.1362	0.4338	18.3	0.9
T2824-1	0.5317	0.1703	0.5583	17.8	1.0
T2824-1A	0.6927	0.214	0.7249	17.1	0.6

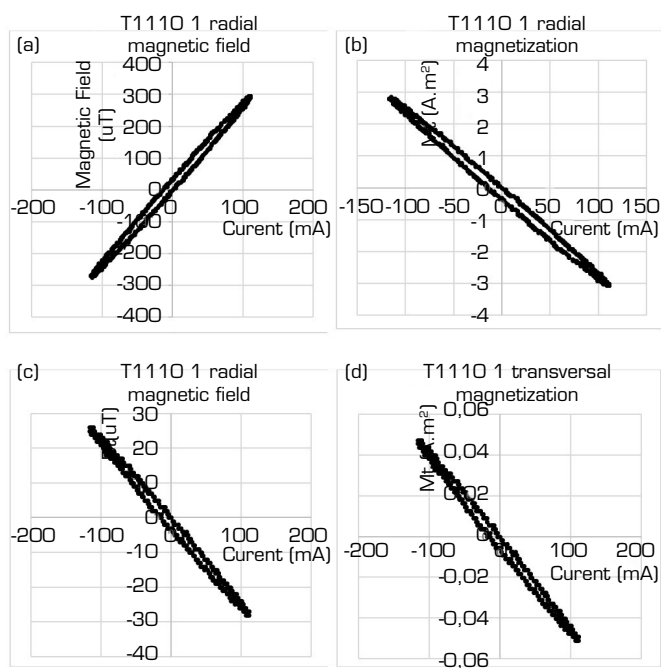
Source: Elaborated by the authors.

The preliminary results from magnetic field and magnetization magnitude measurements (Table 3), alongside the magnetic field versus applied current and magnetization versus applied current curves (Figs. 11–14), can be summarized as follows:

- Torquers featuring a FINEMET core (T0100-1, T1110-1, T2824-1) exhibit less pronounced hysteresis curves, indicating a more linear actuation desirable for satellite attitude control systems. This is a significant advantage as it reduces the need for employing demagnetization techniques (Soares *et al.* 2023).
- Among these prototypes with a nanocrystalline core, T0100-1 demonstrates the most favorable magnetization-to-mass ratio at  $4.959 \times 10^{-3}$ , surpassing T1110-1 at  $3.476 \times 10^{-3}$  and T2824-1 at  $4.365 \times 10^{-3}$ . The ratio for T2824-1A (FeNi50) is  $4.868 \times 10^{-3}$ .
- Regarding the magnetization value, the prototype with a FeNi50 core demonstrates superior performance. However, this device exhibits a more pronounced hysteresis curve, resulting in more non-linear behavior, potentially posing challenges for attitude control applications.

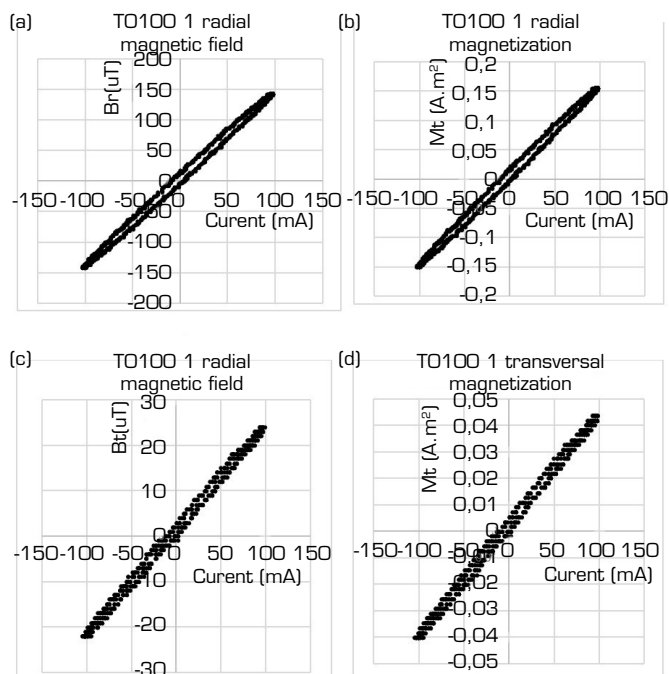
The prospect for further development of prototypes for embedded flight tests would involve enhancements in device construction, alongside systematic and repetitive measurements to accumulate a larger dataset, allowing rigorous statistical analysis for appropriate device qualification.





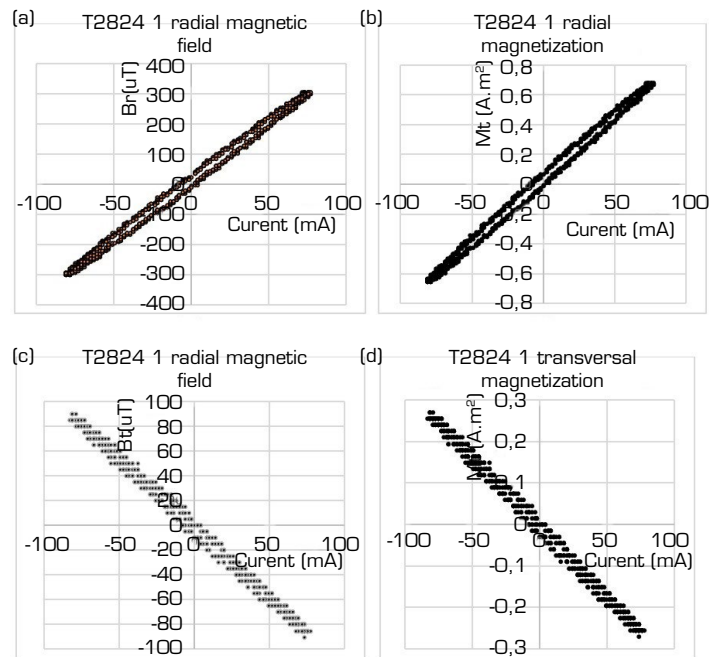
Source: Elaborated by the authors.

**Figure 11.** Magnetic field measurements on torquer T1110-1: (a) radial field; (b) magnetization in the radial direction; (c) transversal field; (d) magnetization in the transversal direction.



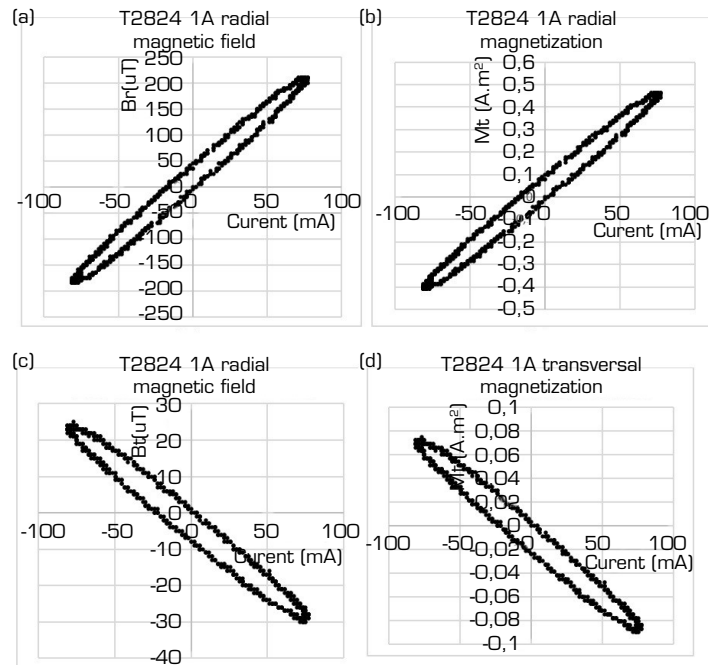
Source: Elaborated by the authors.

**Figure 12.** Magnetic field measurements on torquer T0100-1: (a) radial field; (b) magnetization in the radial direction; (c) transversal field; (d) magnetization in the transversal direction.



Source: Elaborated by the authors.

**Figure 13.** Magnetic field measurements on torquer T2824-1: (a) radial field; (b) magnetization in the radial direction; (c) transversal field; (d) magnetization in the transversal direction.



Source: Elaborated by the authors.

**Figure 14.** Magnetic field measurements on torquer T2824-1A: (a) radial field; (b) magnetization in the radial direction; (c) transversal field; (d) magnetization in the transversal direction.



## CONCLUSION

The constraints from the implementation of axiomatic design imply that the number of turns, resistance, and wire length are directly proportional to the number of layers and inversely proportional to the wire diameter. An increase in the number of layers necessitates more turns to complete all layers, leading to an increase in wire length and, consequently, wire resistance. Conversely, increasing the wire diameter reduces the number of turns required per layer, thereby decreasing wire length and resistance. The behavior of the current reveals inverse tendencies. An increase in wire diameter requires a higher electron density per unit area, leading to an increase in the required current. However, an increase in the number of layers results in a reduction in the required current. In this model, the saturation induction is 27.8 mT, which is achieved when the solenoid generates a magnetic field with a magnitude of 1005 A/m. The hypothesis regarding the benefits of applying axiomatic design theory finds support in the enhanced procedures for selecting multiple design parameters of these magnetic devices, leveraging the interconnectivity and non-independent variation of these parameters.

Another objective involves the innovative selection of material for the magnetorquer core: a nanocrystalline alloy, FINEMET, aimed at achieving improved activation behavior, i.e., a more linear response conducive to effective attitude control systems. While the FeNi50 alloy core exhibited higher magnetization, the results from the nanocrystalline material highlight the potential for developing a more efficient device, particularly in addressing hysteresis activation issues. In summary, the test results of the proposed device designs demonstrate contrasting performance with respect to core material: while the use of nanocrystalline material offers superior hysteresis characteristics or linearity behavior, the FeNi50 alloy demonstrates enhanced magnetization magnitude.

Future studies should consider efforts to produce bars in smaller dimensions and more suitable formats to further enhance performance. Moreover, additional experimental tests are required to qualify and validate the design improvements. Measurements of magnetic dipole moment, required current, and wire resistance are inherently linked to analyze necessary modifications to the design model. Measuring the variation of induction with current will enable the construction of a hysteresis cycle for the core material and facilitate comparison of saturated induction levels. An alternative approach involves developing a method to calculate the ratio of turns per layer, considering manufacturing non-uniformities that may reduce the ratio as the number of layers increases.

## CONFLICT OF INTEREST

Nothing to declare.



## AUTHOR'S CONTRIBUTION

**Conceptualization:** Martins-Filho LS, Soares MA, Gueron E, Ferreira ES, and Morsch HO; **Methodology:** Martins-Filho LS, Soares MA, Gueron E, Ferreira ES, and Morsch HO; **Investigation:** Martins-Filho LS, Soares MA, Gueron E, Ferreira ES and Morsch HO; **Writing – Original Draft:** Martins-Filho LS, Soares MA, and Gueron E; **Writing – Review and Editing:** Martins-Filho LS, Soares MA, and Gueron E; **Supervision:** Martins-Filho LS and Gueron E; **Final approval:** Martins-Filho LS.

## DATA AVAILABILITY STATEMENT

All data sets were generated and analyzed in the current study.

## FUNDING

Fundação de Amparo à Pesquisa do Estado de São Paulo   
Grant No: #2019/06174-7.  
Conselho Nacional de Desenvolvimento Científico e Tecnológico 

## ACKNOWLEDGMENTS

<https://ror.org/03swz6y49>

## REFERENCES

- [ASTM] American Society for Testing and Materials (2018) ASTM B258-18: standard specification for standard nominal diameters and cross-sectional areas of AWG sizes of solid round wires used as electrical conductors. ASTM International. <http://doi.org/10.1520/B0258-18>
- [NASA] National Aeronautics and Space Administration (1969) Spacecraft magnetic torques. NASA, Washington DC (United States). Technical Report NASA SP-8018.
- Cal Poly (2020) CubeSat design specification Rev. 14. [accessed Apr 15 2021]. <https://www.cubesat.org/cds-announcement>
- Carrara V, Varotto SEC (1995) Projeto de bobinas magnéticas para uso em satélites. Instituto Nacional de Pesquisas Espaciais (INPE), São José dos Campos, SP (Brazil). Technical Report INPE-5665-NTC-319.
- Coutinho DA, Paulino PSL, Conceição AA, Vilela SF, Aquino GP, Ferreira-Junior AA, Vilas Boas EC (2023) Design, prototyping and stratospheric launch of CubeSats for university competition. *J Aerosp Technol Manag* 15: e0623. <https://doi.org/10.1590/jatm.v15.1295>
- Duarte RO, Vale SRC, Martins-Filho LS, Torres FE (2020) Development of an autonomous redundant attitude determination system for Cubesats. *J Aerosp Technol Manag* 12: e3020. <https://doi.org/10.5028/jatm.v12.1166>
- Farrahi A, Sanz-Andre´ SA (2013) Efficiency of hysteresis rods in small spacecraft attitude stabilization. 2013: 45957. <https://doi.org/10.1155/2013/459573>
- Feynman RP, Leighton RB, Sands M (2012) The Feynman lectures on physics. 3rd ed. Vol. 2. London: Pearson.
- Gerhardt DT, Palo SE (2010) Passive magnetic attitude control for CubeSat spacecraft. Paper presented 24th Annual AIAA/USU Conference on Small Satellites. AIAA/USU; Logan, USA.
- Gheiratmand T, Hosseini HRM (2016) Finemet nanocrystalline soft magnetic alloy: investigation of glass forming ability, crystallization mechanism, production techniques, magnetic softness and the effect of replacing the main constituents by other elements. *J Magn Magn Mater* 408:177-192. <https://doi.org/10.1016/j.jmmm.2016.02.057>
- Hitachi Metals Ltd. (2016). FINEMET Catalog 2016. Tokyo: Hitachi.
- Lee J, Ng A, Jobanputra R (2002) On determining dipole moments of a magnetic torquer rod – Experiments and discussions. *Can Aeronaut Space J* 48(1): 61-67. <http://doi.org/10.5589/q02-014>



Lee S-H, Seo H-H, Rhee S-W (2005) Performance analysis of magnetic torquer for spacecraft control. Paper presented International Conference on Control, Automation, and Systems. ICCAS; Gyeonggi-Do, Korea.

Lincoln Lab (1965) Design of electromagnetic torquer rod. Massachusetts Institute of Technology (MIT), Cambridge MA (United States). Report ESD-TDR-65-589.

Markley FL, Crassidis JL (2014) Fundamentals of spacecraft attitude determination and control. New York: Springer.

Mehrjardi MF, Mirshams M (2010) Design and manufacturing of a research magnetic torquer rod. *Contemp Eng Sci* 3(5): 227-236. <https://doi.org/10.1117/12.851652>

Ousaloo HS (2013) Hysteresis nutation damper for spin satellite. *The Open Aerospace Engineering Journal* 6:1-5. <http://doi.org/10.2174/1874146001306010001>

Perondi LF (2023) The coming of age of space satellite industry: transitioning from a growth to a maturity life cycle. *J Aerosp Technol Manag* 15: e0323. <https://doi.org/10.1590/jatm.v15.1291>

Pessoa-Filho JB (2021) Space age: past, present and possible futures. *J Aerosp Technol Manag* 13: e3421. <https://doi.org/10.1590/jatm.v13.1226>

Roohnavazfar M, Houshmand M, Zarandi RN, Mirsalim M (2014) Optimization of design parameters of a limited angle torque motor using analytical hierarchy process and axiomatic design theory. *Prod Manuf Res* 2(1): 400-414. <https://doi.org/10.1080/21693277.2014.904762>

Santoni F, Zelli M (2009) Passive magnetic attitude stabilization of the UNISAT-4 microsatellite. *Acta Astronautica* 65(5-6): 792-803. <https://doi.org/10.1016/j.actaastro.2009.03.012>

Sato M, Ishii Y (1989) Simple and approximate expressions of demagnetizing factors of uniformly magnetized rectangular rod and cylinder. *J Appl Phys* 66(2): 983-985. <https://doi.org/10.1063/1.343481>

Schaeffer L, Espinoza FRM (2000) Magnetic properties of mechanically alloyed Fe50% Ni. *Braz J Mater Sci Eng* 2(3):19-28.

Soares MA, Martins-Filho LS, Baroni L, Durão OSC, Schad V (2023) Attitude determination and control of a nanosatellite detector of cosmic sources of X and gamma rays. Paper presented 2023 27th International Congress of Mechanical Engineering. COBEM; Florianopolis, Brazil. <http://doi.org/10.26678/ABCM.COBEM2023.COB2023-0647>

Suh NP (1990) *The principles of design*. New York: Oxford University.

Suh NP (1995) Designing-in of quality through axiomatic design. *IEEE Trans Reliabi* 44(2): 256-264 <https://doi.org/10.1109/24.387380>